Available online at www.sciencedirect.com
SCIENCE DIRECT®
Journal of Sound and Vibration 264 (2003) 579–603
JOURNAL OF SOUND AND VIBRATION
www.elsevier.com/locate/jsvi

Dynamic response of doubly curved honeycomb sandwich panels to random acoustic excitation. Part 1: Experimental study

P.R. Cunningham*, R.G. White

School of Engineering Sciences, Aeronautics and Astronautics, University of Southampton, Highfield, Southampton, Hampshire SO17 1BJ, UK

Received 6 August 2001; accepted 26 June 2002

Abstract

A set of four doubly curved, composite honeycomb sandwich panels has been tested with broad band, random acoustic excitation in a progressive wave tube facility. This paper presents the experimental results in the form of dynamic face plate strain measurements taken from various points close to the centre of the panels, on both the inner and outer face plates. The panels were tested at overall sound pressure levels up to 164 dB (ref. 2×10^{-5} Pa, over a frequency bandwidth of 60–600 Hz). The response was found to be linear, with a maximum measured root mean square strain of 250με. The doubly curved geometry was found to have a profound effect on the ratio of inner-to-outer face plate strain, which was compared with ratios reported for flat and singly curved geometries. The second part of this study concentrates on three methods for predicting the response of the doubly curved panels to random acoustic excitation.

1. Introduction

The dynamic response of aircraft structures to random pressure loading from aerodynamic and engine acoustic sources can lead to acoustic fatigue failures [1–7] and it is the understanding of these acoustic sources, coupled with the development of structural response prediction models, which will enable the engineer to design against acoustic fatigue. Since the introduction of the gas turbine engine, and its development from the early turbojet to the modern high bypass turbofans of today, the acoustic fatigue of aircraft structures has remained an important design issue. Much work has been carried out over the years in an attempt to predict the stresses that could be

*Corresponding author. Tel.: +44-23-8059-4887; fax: +44-23-8059-3058.
E-mail address: prc1@soton.ac.uk (P.R. Cunningham).

0022-460X/03/$ - see front matter
PII: S0022-460X(02)01210-5

encountered in service due to the random acoustic loading produced by the gas turbine engine [8–11]. However, with the introduction of advanced composite materials, a new set of issues have had to be addressed which concern the very different fatigue characteristics of this new type of structure [4].

One particular type of composite structure, the honeycomb sandwich panel, has a very high stiffness-to-weight ratio, and has found favour in the aircraft industry over the years. Panels employing a mixture of carbon fibre reinforced plastics and resin impregnated paper honeycomb can be found in applications such as fairings and floor panels, ailerons, helicopter rotor blades, and engine intake barrel panels. The latter type of structure has a complicated geometry due to the shape of the engine intake, and as such can be considered to be doubly curved. The dynamic response of sandwich structures to acoustic excitation has previously been investigated [12–15], but only for flat and singly curved geometries.

In this paper, which is the first in a two-part study, results are presented from a recent experimental study conducted at the University of Southampton. In the previous work, the free vibration of doubly curved, composite honeycomb sandwich panels was investigated, and finite element models of the panels have been validated [16]. The study is extended to investigate the dynamic response of a set of doubly curved, honeycomb sandwich structures to high intensity, random acoustic excitation using a progressive wave tube facility. The panels were tested at overall sound pressure levels (OASPLs) up to 164 dB (ref. 2×10^{-5} Pa, frequency bandwidth 60–600 Hz), and overall root mean square (r.m.s.) strains were recorded from the inner or concave (facing) and outer or convex (backing) skins in order to make comparisons with the theoretical prediction of the response, which is covered in Part 2 of this study. The measured ratio of inner-to-outer face plate strain was compared with similar results for flat and singly curved geometries [17,18], and conclusions are drawn with regard to the effect of the degree of double curvature on this ratio.

2. Experimental set-up

The ISVR progressive wave tube facility, shown in Fig. 1, uses a Wyle Labs WAS 3000 air modulator as the acoustic source. The WAS 3000 is an electro-pneumatic device which has a maximum acoustical power output of 30 kW over a frequency range 25–10 kHz. Air modulation is achieved by using the principle of a vibrating vane to produce pressure fluctuations in the supply air stream. When coupled to an exponential horn, maximum OASPLs of 164 dB (ref. 2×10^{-5} Pa) can be achieved with a frequency range of 60–600 Hz. The PWT facility has a working section which is 1.2 m long, 0.6 m high, and 0.3 m deep. Panels are secured in an appropriate test fixture which is then bolted into the test aperture to form one wall of this section. The panels are therefore excited by grazing incidence sound which propagates along the PWT where it is finally attenuated in the noise attenuation duct downstream of the test section.

An important aspect of a PWT is the spatial variation in sound pressure level and the degree of coherence of the sound field around the test section. This has been investigated by a previous researcher [19] for the PWT used for these tests. In this study, a 25 mm thick plywood board with seven holes drilled to take a B&K microphone (two upstream, two downstream, and three in the cross-sectional plane of the tunnel reference microphone) was used to blank the PWT aperture, as

shown in Fig. 2. Two microphones were used in this study (one for the tunnel reference location, and one which was moved around each of the seven locations in the plywood board) therefore the measurements of coherence around the aperture were all relative to the tunnel reference microphone. Tests were carried at OASPLs from 140 to 160 dB in 5 dB steps, and seven measurement were taken per OASPL level, taking care to ensure the OASPL was at a constant level between tests. The results showed a reasonable coherence between the reference location and each of the seven panel locations, with a drop in coherence at OASPLs above 150 dB [19]. Table 1 shows a comparison of measured OASPL compared with the measured reference level at each of

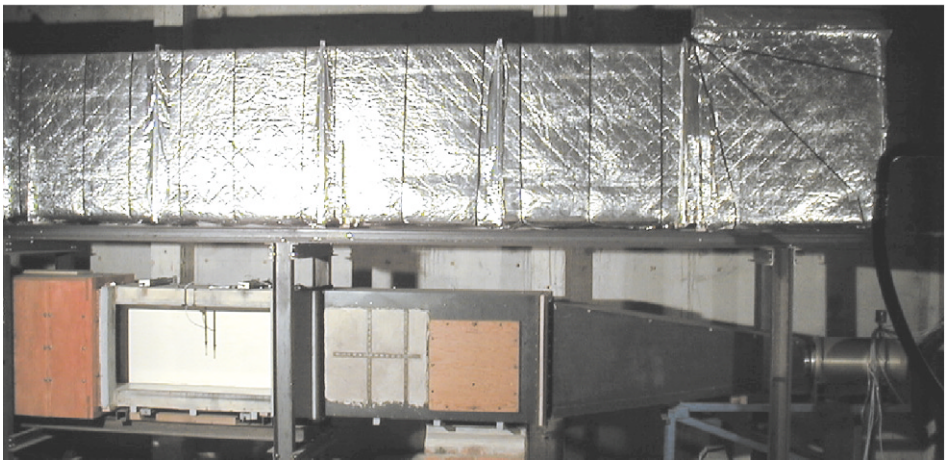

Fig. 1. The ISVR progressive wave tube facility.

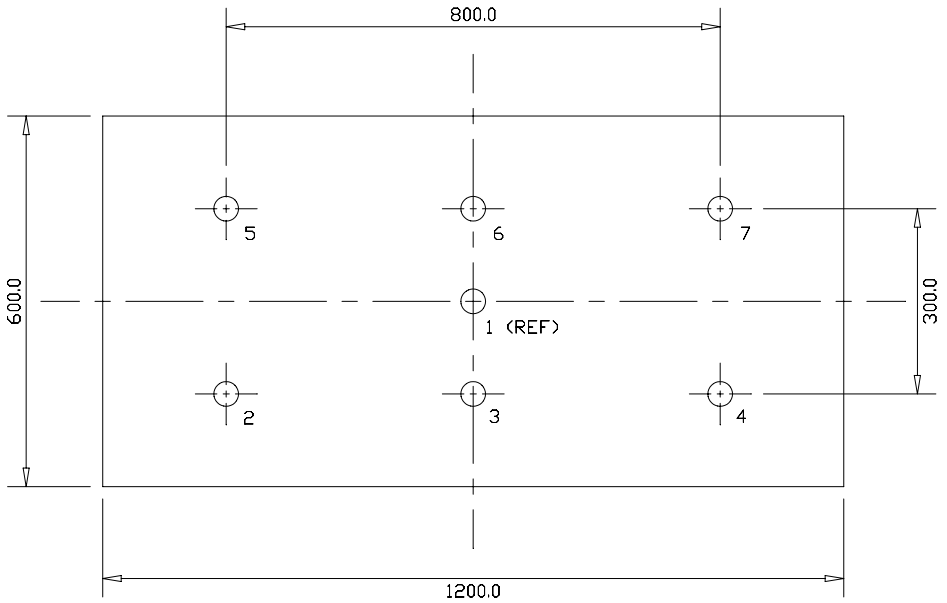

Fig. 2. Microphone positions used to ascertain the spatial variation in sound pressure level [19].

the seven panel locations. As can be seen, the maximun variation along the axis of the aperture was 3.1 dB and from the bottom to the top of the aperture the maximum variation was 2.9 dB. The tests also confirmed the presence of travelling waves along the duct, by reference to the phase between each measurement location on the board and the reference microphone in the tunnel aperture. The phase spectra relative to the reference microphone for panel microphones 5 and 7 are plotted together in Fig. 3. As can be seen, there is a frequency at which both microphones appear to be in phase relative to the reference microphone, which in this case is $\approx$428.5 Hz. At this frequency, the wavelength should be equal to the distance between the two microphones, i.e.,

Table 1
Spatial variation of measured OASPL in the PWT aperture

OASPL (dB)	Test number/panel microphone position													
	1		2		3		4		5		6		7	
	Measured OASPL (dB)													
	Ref.	Panel	Ref.	Panel	Ref.	Panel	Ref.	Panel	Ref.	Panel	Ref.	Panel	Ref.	Panel
140	144.9	142.9	145.1	143.7	144.5	141.8	145.6	142.2	144.9	142.3	144.5	144.7	143.9	141.4
145	149.8	147.5	150.2	149.1	149.8	147.3	151.4	149.0	150.4	150.1	152.1	151.2	151.5	148.9
150	155.8	154.2	155.5	154.9	156.6	154.2	155.9	154.5	156.1	155.7	155.9	156.4	155.6	153.8
155	160.8	158.4	160.9	161.2	161.4	158.1	160.6	159.1	161.2	161.7	161.4	159.9	159.9	157.6
160	165.9	164.4	165.3	166.7	165.8	164.9	165.7	164.7	166.1	167.1	164.8	164.8	166.7	165.9

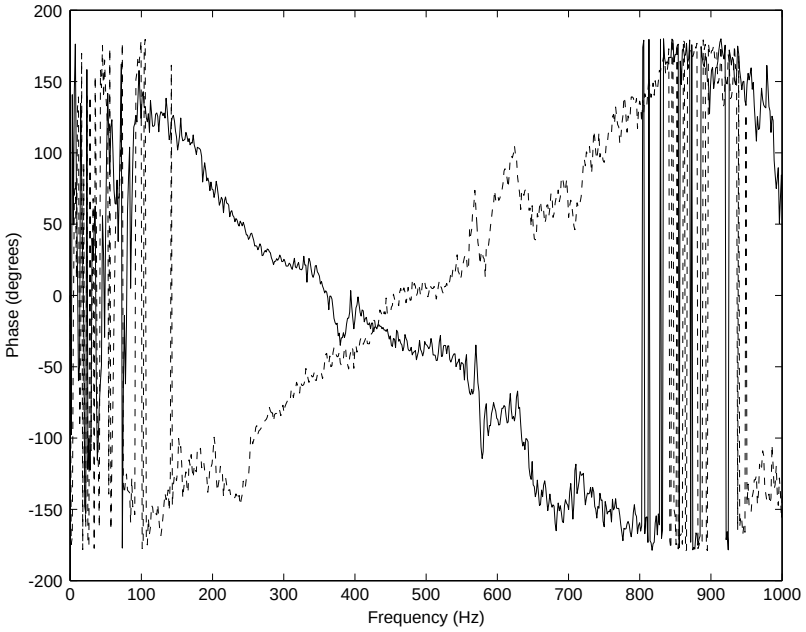

Fig. 3. Phase spectra for panel microphones 5 (–) and 7 (- -) at 150 dB OASPL.

0.8 m, and using the relationship between wavelength and frequency, $c = \lambda f$, the wavespeed, c, is found to be equal to 342.8 m/s, which is approximately the speed of sound in air [19].

The test panels consisted of four doubly curved, composite honeycomb sandwich panels with identical plan area and different radii of curvature. Panels 1–3 were designed with a symmetric sandwich lay-up (i.e., equal number of layers in both face plates) and panel 4 was designed with an asymmetric sandwich lay-up. The panels were designed and manufactured at the University of Southampton using SP Systems SE84/RC200P/1000/42 epoxy resin pre-impregnated plain weave carbon cloth for the face plates and Hexcel Aeroweb A1-48-5 OX lightweight resin impregnated honeycomb for the core. Details of the dimensions and radii of curvature of each panel, the lay-up details, and the material properties are given in Tables 2, 3 and 4, respectively, and in Fig. 4, and the mass per unit area of each panel was found to be approximately 5.24 kg/m^2 for all four panels. A full description of the design and manufacture of the panels can be found in Ref. [16].

The experimental set-up is shown in Fig. 5. A B&K Type 1402 random signal generator was used to supply the drive signal, which was attenuated outside the 60–600 Hz range using a B&K Type 5612 spectrum shaper. The signal from the shaper was amplified using a B&K Type 2608 measuring amplifier before being supplied to the LDS PA 500L power amplifier in order to give the required range to drive the WAS 3000 at the high sound pressure levels. The OASPL in the test section was monitored using a B&K Type 4136 condenser microphone coupled to a B&K Type 2609 measuring amplifier with the appropriate scale fitted. A Measurements Group model 2200 signal conditioning amplifier was used to calibrate and amplify the signals from the strain gauges, which were filtered at 1 kHz using a 16 channel low-pass filter set. The signals were then digitally sampled using a National Instruments VXI data acquisition system coupled to a personal computer. In addition to the strain gauges, two B&K Type 4344 accelerometers were used to measure the dynamic response of the panels. The signals from the accelerometers were conditioned using B&K Type 2635 charge amplifiers before being filtered and digitally sampled.

2.1. Panel attachment in the PWT aperture

The design and manufacture of a suitable test fixture for the doubly curved panels is a very difficult task when one considers the geometry and stiffness of the panel itself, and the need to accurately model the panels in the PWT using the finite element method. One of the main objectives of the work reported in this two-part study was to predict the responses of the test panels to random acoustic excitation and compare these with experimental results obtained from the PWT tests. It was important that the highest possible strain was achieved in order that

Table 2
Dimensions for the experimental test panels

Panel	Plan dimensions		Radii of curvature	
	x (m)	y (m)	R_x (m)	R_y (m)
1	0.912	0.525	3.5	1.0
2	0.912	0.525	1.2	1.0
3	0.912	0.525	3.5	0.5
4	0.912	0.525	3.5	0.5

Table 3
Ply lay-up details for the experimental test panels (panel 4 in parentheses)

Layer	Number of plies	Ply orientation
Facing skin	4 (2)	$[0/45]_s$
Doublers	2	[0/30]
Spacers	2	$[0_2]$
Edge pan	3	[0/45/0]
Backing skin	4 (6)	$[0/45]_s$

Table 4
Material specifications for the experimental test panels

Layer	Thickness (m)	Elastic modulus (Pa)		Shear modulus (Pa)				Density (kg/m^3)	Poisson ratio
		E_{11}	E_{22}	E_{33}	G_{12}	G_{xz}	G_{yz}		
CFRP[a]	0.25e–3	57.93e9	57.93e9	—	3.7e9	—	—	1518.0	0.04
Honeycomb	19.0e–3	0	0	120e6	0	35e6	20e6	48.0	—

[a] Properties obtained using cured test specimens with $[0_4]$ and $[45_4]$ ply lay-up and with 60% fibre volume fraction.

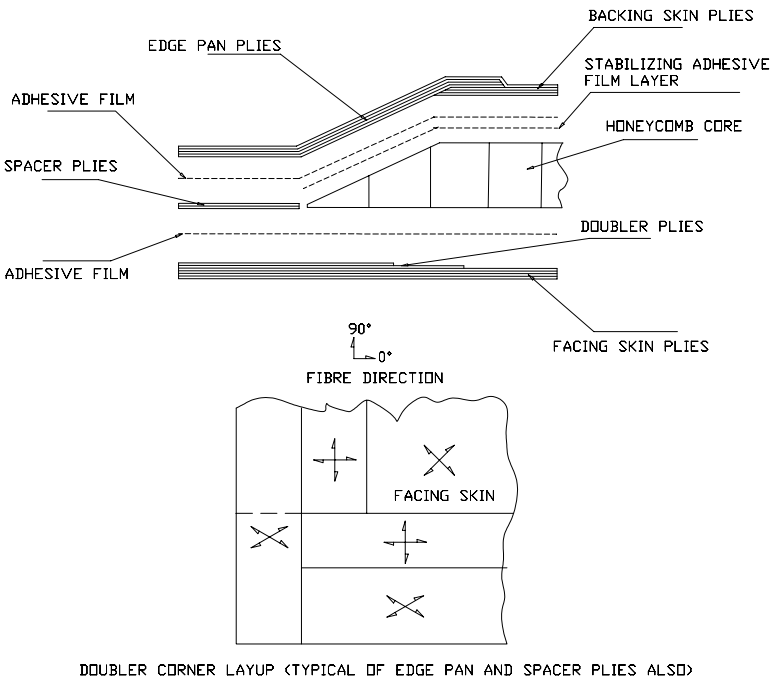

Fig. 4. Bevelled edge and lay-up detail.

potential non-linear effects could be investigated. In addition, the panels and associated boundary conditions in the PWT needed to be modelled as accurately as possible so that a representative comparison between test and theory could be made.

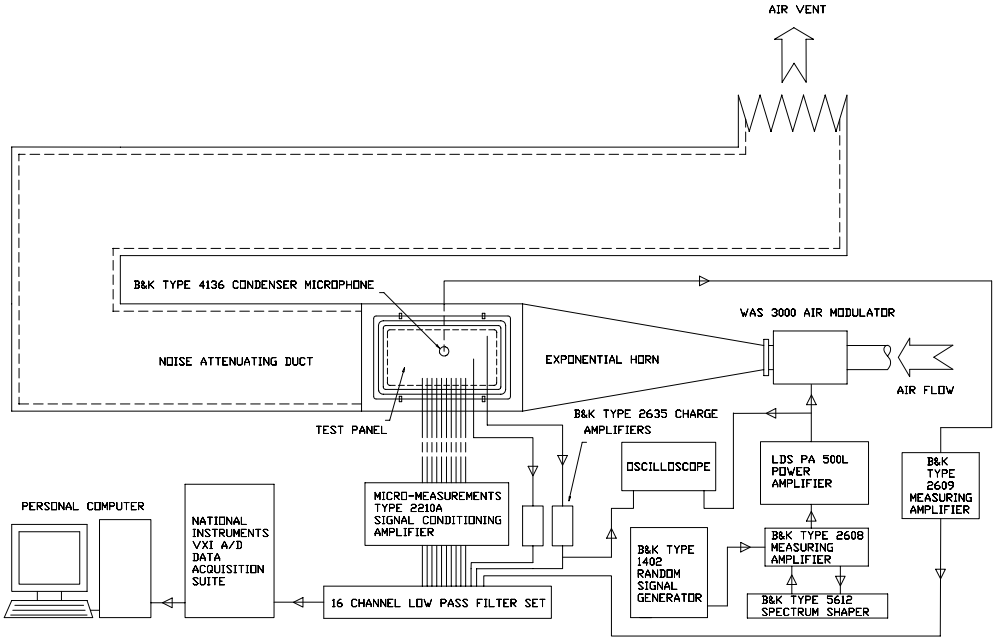

Fig. 5. Experimental set-up of the panels in the PWT facility.

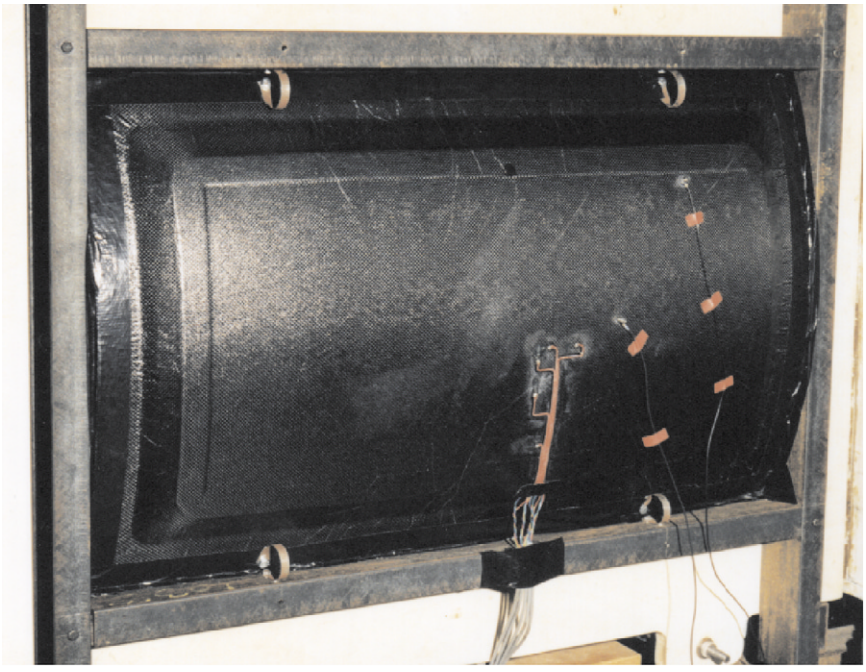

Fig. 6. Panel 3 secured in the PWT aperture using four circular steel springs.

Initial test fixture designs centred around moulding a glass fibre/epoxy "picture" frame. The problem with this approach was two-fold. This type of test fixture would introduce extra stiffness which would result in a very low-level strain response, and an increase in the predominant response frequency which could be outside the broadband frequency limits of the PWT facility (80–800 Hz). Secondly, the best way to manufacture this fixture would be to use the panel as a mould and use the wet lay-up method. However, this method would produce a fixture with variable thickness and poor quality consolidation. To this end, each panel was secured in the test aperture of the PWT using four circular steel springs, as shown in Fig. 6. The circular springs introduce very little extra stiffness to the panel, thus allowing the highest possible strain to be achieved. In addition, the natural frequencies of vibration and the associated modes were very close to that of the freely supported test panel [16], which was verified using a finite element model of the configuration and comparing this with the experimental results for the freely supported test panels, as shown in Table 5. The spring stiffness in the out-of-plane (transverse) direction was approximately 7400 N/m per spring, which results in a transverse rigid-body mode of vibration with a resonant frequency in the region of 19 Hz.

Table 5
Comparison of measured (from the freely supported and PWT tests) and predicted resonance/natural frequencies of the four test panels

Measured (Free) (Hz)	Measured (PWT) (Hz)	ANSYS results (Chamfered edge model with spring supports) (Hz)
Panel 1		
136.0	—	141.14
214.6	210.48	219.02
282.6	—	282.61
352.1	353.9	357.93
Panel 2		
131.5	—	136.49
164.7	163.1	164.30
269.0	—	267.28
343.1	330.8	338.22
Panel 3		
130.9	—	137.65
264.5	258.9	272.62
280.9	—	300.31
320.4	320.7	335.08
Panel 4		
74.65	—	82.39
233.18	—	251.13
279.26	269.6	288.67
312.44	315.2	319.28

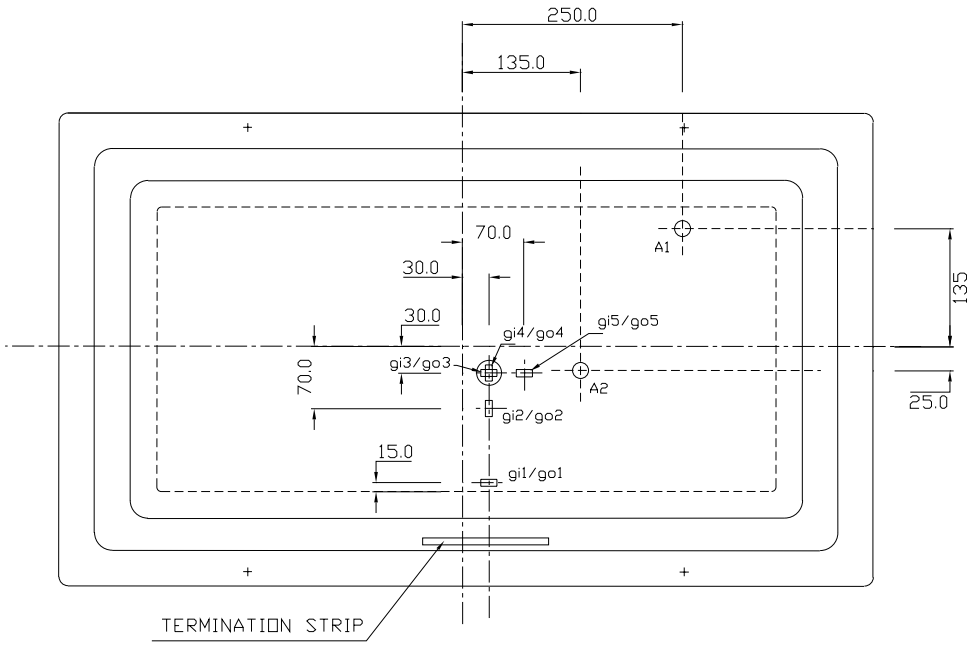

Fig. 7. Strain gauge and accelerometer locations.

2.2. Strain gauge locations

Single-element gauges and tee-rosette gauges, each with a gauge length of 6 and 5 mm, respectively, a nominal resistance of $120 \pm 0.5\Omega$, and a gauge factor of 2.1, were used to measure the dynamic response of the test panels. All of the gauges were wired into quarter bridge circuits, which were incorporated in the Measurements Group 2200 signal conditioning amplifier. Since long leads were used from the strain gauges to the measuring amplifier situated in the control room, three wire connection was used to eliminate dc offset and balancing problems. For the spring-supported test panels, the gauges were located on the inner and outer face (concave and convex face, respectively) of the test panels at the locations shown in Fig. 7.

3. Testing procedure

Testing was carried out at OASPLs from 140 to 160 dB in 5 dB steps. The driving signal to the WAS 3000 was attenuated outside the 60–600 Hz frequency range using a B&K Type 5612 spectrum shaper [20] as previously mentioned. Five tests were carried out for each panel in order to assess the repeatability of the experiments.

Initial calibration of the strain gauges was carried out using the internal shunt circuit in the signal conditioning amplifier, which creates a dummy strain of 1000με across the bridge. An excitation voltage of 2 V was used and the gauges were calibrated to give 2 V output at 1000με. Before each test, the strain gauges were balanced.

Table 6
Statistical properties for panel 1 subject to random acoustic excitation in the PWT

OASPL (dB)	Mic. (Pa)	Acc.1 ($N\,m^{-1}s^2$)	Acc.2 ($N\,m^{-1}s^2$)	gi1 (με)	gi2 (με)	gi3 (με)	gi4 (με)	gi5 (με)	go1 (με)	go2 (με)	go3 (με)	go4 (με)	go5 (με)
Mean													
143.29	−6.19	−0.0002	0.0003	5.45	2.28	14.18	17.80	8.46	0.91	13.59	10.39	5.57	5.14
149.97	−5.96	−0.0003	0.0003	0.42	−0.20	14.24	16.40	4.95	6.09	18.70	16.88	12.83	11.72
154.75	−5.91	−0.0002	0.0003	−5.42	−4.64	10.31	10.62	−1.01	4.71	15.68	13.39	9.63	10.48
159.28	−6.02	−0.0002	0.0005	−7.66	−5.72	9.28	9.25	−2.37	4.45	14.28	12.51	9.15	10.05
163.71	−5.95	−0.0002	0.0003	−3.14	2.06	16.32	14.09	3.78	7.97	14.16	12.37	12.90	13.49
Standard deviation (*r.m.s.*)													
143.29	292.33	0.005	0.011	8.99	11.95	12.73	6.78	5.63	15.75	9.77	10.97	16.53	14.72
149.97	630.51	0.011	0.022	18.27	26.47	28.31	13.49	10.90	34.58	21.25	24.10	36.57	31.39
154.75	1092.30	0.020	0.038	31.94	46.77	50.11	22.36	18.88	61.36	37.40	42.42	64.65	55.23
159.28	1842.24	0.034	0.065	55.38	80.90	86.62	36.53	32.63	107.22	64.31	73.04	112.11	95.55
163.71	3066.80	0.062	0.115	99.81	145.58	154.84	66.77	59.67	196.01	113.75	128.39	203.04	173.13
Skewness (*zero mean*)													
143.29	0.023	−0.010	0.003	−0.053	0.008	0.010	0.160	0.003	−0.005	−0.013	−0.025	0.004	0.009
149.97	0.044	0.032	0.020	−0.015	0.007	−0.003	0.290	−0.026	0.011	−0.035	−0.026	−0.003	−0.015
154.75	−0.048	0.054	0.062	−0.056	−0.001	−0.016	0.298	−0.048	0.003	−0.005	−0.007	−0.012	−0.010
159.28	−0.059	0.067	0.047	−0.113	0.020	−0.007	0.163	−0.106	0.021	−0.037	−0.032	0.004	0.005
163.71	−0.065	0.138	0.077	−0.211	0.045	0.003	−0.050	−0.231	0.045	−0.069	−0.050	−0.003	0.004
Kurtosis (*zero mean*)													
143.29	6.21	3.44	3.40	3.36	3.45	3.48	3.67	3.17	3.46	3.44	3.43	3.50	3.45
149.97	5.02	3.29	3.37	3.38	3.39	3.40	3.46	3.36	3.44	3.38	3.38	3.43	3.42
154.75	3.88	3.21	3.26	3.02	3.07	3.06	3.15	3.07	3.03	3.05	3.04	3.05	3.05
159.28	3.42	3.23	3.31	2.98	2.99	3.00	3.14	3.02	2.96	2.99	2.99	2.98	2.99
163.71	2.71	3.11	3.07	3.22	3.22	3.20	3.35	3.26	3.17	3.20	3.18	3.20	3.20

During the operation of the PWT, the air pressure supply to the siren was kept constant at 15 psi for all OASPLs up to 160 dB, at which point the pressure was increased to 20 psi, which gave approximately an extra 2 dB needed to reach an OASPL of 160 dB. The signals from the strain gauges, accelerometers, and microphone were digitally sampled using the National Instruments VXI acquisition suite coupled to a personal computer. A sampling frequency of 6000 Hz was used and 60 000 samples were acquired giving 10 s of data per OASPL. The digital data was saved to disk, ready for post-processing in the MATLAB environment.

4. Experimental results

The statistics of the strain responses of the four doubly curved panels are given in Tables 6–9, and a typical plot of the probability density function of the strain signal from one of the gauges on each panel is shown in Fig. 8. As can be seen, the measured strain moments were very close to that

Table 7
Statistical properties for panel 2 subject to random acoustic excitation in the PWT

OASPL (dB)	Mic. (Pa)	Acc.1 ($N\,m^{-1}s^2$)	Acc.2 ($N\,m^{-1}s^2$)	gi1 (με)	gi2 (με)	gi3 (με)	gi4 (με)	gi5 (με)	go1 (με)	go2 (με)	go3 (με)	go4 (με)	go5 (με)
Mean													
143.88	−7.20	−0.0004	0.0004	2.80	−4.59	−1.41	7.49	10.40	−0.25	8.58	−1.30	−6.35	−3.95
149.91	−6.96	−0.0004	0.0003	15.67	6.90	9.45	19.61	22.28	−2.36	5.31	−5.78	−9.73	−5.93
154.92	−6.95	−0.0004	0.0003	25.22	14.86	17.30	28.85	31.37	−2.53	4.52	−6.04	−9.76	−5.87
159.00	−6.90	−0.0004	0.0003	34.19	22.65	24.82	37.03	39.33	−2.05	4.44	−5.51	−8.35	−4.73
163.09	−7.12	−0.0004	0.0003	49.81	35.02	37.02	52.63	54.80	−2.25	4.89	−4.12	−7.10	−3.90
Standard deviation (*r.m.s.*)													
143.88	313.01	0.005	0.007	7.44	8.49	8.02	6.63	7.02	10.21	7.27	6.25	9.06	9.29
149.91	625.59	0.011	0.014	13.11	16.87	15.88	12.77	13.34	20.46	14.29	12.27	17.92	16.94
154.92	1114.26	0.022	0.027	20.73	27.27	25.64	20.60	21.59	33.09	23.29	20.18	28.71	26.70
159.00	1783.04	0.039	0.049	35.27	46.85	44.02	35.37	37.11	57.13	40.60	35.26	49.47	45.72
163.09	2857.02	0.067	0.082	59.50	78.95	74.15	59.63	62.14	96.65	69.03	60.26	83.62	76.81
Skewness (*zero mean*)													
143.88	−0.029	0.031	−0.006	−0.058	−0.002	−0.001	0.023	0.028	−0.012	−0.006	−0.004	−0.009	0.031
149.91	−0.113	0.100	−0.012	−0.035	0.011	0.005	−0.010	−0.046	0.018	0.018	0.028	0.013	0.035
154.92	−0.147	0.077	−0.025	−0.013	−0.017	−0.019	0.005	0.017	−0.006	0.034	0.045	0.003	−0.004
159.00	−0.127	0.061	−0.036	−0.051	0.037	0.034	−0.043	−0.073	0.040	−0.009	0.004	0.031	0.050
163.09	−0.221	0.009	−0.035	−0.032	−0.011	−0.015	−0.034	−0.022	0.003	0.013	0.025	0.000	−0.016
Kurtosis (*zero mean*)													
143.88	5.31	3.58	3.40	3.14	3.26	3.23	3.18	3.13	3.24	3.23	3.21	3.19	3.17
149.91	4.41	3.40	3.24	3.11	3.12	3.11	3.14	3.14	3.12	3.15	3.16	3.13	3.15
154.92	3.76	3.24	3.23	3.02	3.01	3.01	3.02	3.06	3.00	3.05	3.08	2.96	2.98
159.00	3.35	3.17	3.24	3.18	3.19	3.19	3.17	3.12	3.20	3.17	3.16	3.21	3.18
163.09	3.10	3.07	3.20	3.21	3.24	3.24	3.22	3.20	3.24	3.23	3.22	3.26	3.24

of a Gaussian distribution with the skewness close to zero and the kurtosis close to three at all sound pressure levels. This clearly shows that the response of the panels was linear at all loading levels. For the measured pressure loading, departure from Gaussianity was evident at the lower sound pressure levels with a high kurtosis values around 4.4–6.2, however the skewness values were still quite low. Fig. 9 shows the same probability density functions given in Fig. 8 (with the addition of the microphone pdf), but with a logarithmic vertical scale to show details of the 2σ to 5σ range. Although there appears to be a departure from the Gaussian distribution in the 2σ to 5σ range, there is no systematic trend with increasing OASPL for both the strain and microphone results presented. The reason for this departure is unknown and further investigation is outside the scope of this paper, however, the results of Fig. 9 are interesting to note.

The digitized time histories of strain, acceleration, and pressure were factored to take account of the gains introduced by the respective measurement amplifiers. The resulting data were then transformed to the frequency domain using the "spectrum" function in the MATLAB environment. A Hanning window was applied to the segmented data, which consisted of 8192

Table 8
Statistical properties for panel 3 subject to random acoustic excitation in the PWT

OASPL (dB)	Mic. (Pa)	Acc.1 ($N\,m^{-1}s^2$)	Acc.2 ($N\,m^{-1}s^2$)	gi1 (με)	gi2 (με)	gi3 (με)	gi4 (με)	gi5 (με)	go1 (με)	go2 (με)	go3 (με)	go4 (με)	go5 (με)
Mean													
143.51	−6.92	−0.0004	0.0003	−1.85	−2.52	5.63	8.71	6.84	6.84	6.57	13.24	3.02	−2.87
149.93	−6.91	−0.0004	0.0003	9.33	7.08	15.13	20.00	18.61	11.36	10.22	16.01	5.48	−3.80
154.18	−6.73	−0.0003	0.0003	17.52	13.79	21.66	27.84	26.99	12.13	11.48	17.80	6.80	−3.48
158.84	−6.73	−0.0003	0.0003	24.45	19.82	27.36	34.81	34.26	12.84	14.01	21.18	9.65	−1.32
162.82	−6.25	−0.0003	0.0002	35.49	29.09	35.80	46.26	46.77	14.31	17.32	26.01	12.80	0.46
Standard deviation (*r.m.s.*)													
143.51	299.76	0.004	0.015	5.06	11.25	11.76	4.57	4.72	8.74	9.95	10.51	10.64	10.51
149.93	627.57	0.009	0.031	8.01	23.74	24.92	9.00	8.80	18.51	21.28	22.66	22.29	20.89
154.18	1023.49	0.016	0.049	12.55	41.13	43.19	14.41	14.02	31.44	36.54	39.23	36.00	33.57
158.84	1751.63	0.028	0.084	21.02	70.72	74.10	24.08	23.67	54.97	61.85	66.87	61.72	56.87
162.82	2768.33	0.047	0.134	34.68	121.65	126.48	38.42	37.78	92.83	103.62	112.50	100.67	92.00
Skewness (zero mean)													
143.51	−0.103	0.031	0.010	−0.054	−0.024	−0.031	0.048	0.052	0.020	0.050	0.055	0.008	0.024
149.93	−0.092	0.030	0.015	−0.046	−0.012	−0.017	0.029	0.034	−0.008	0.042	0.045	−0.020	−0.010
154.18	−0.074	0.080	0.012	−0.017	0.004	0.000	0.004	0.016	0.005	0.020	0.016	0.002	0.009
158.84	−0.111	0.079	0.019	−0.054	−0.019	−0.029	0.042	0.065	−0.014	0.050	0.054	−0.026	−0.018
162.82	−0.161	0.037	0.031	−0.070	−0.018	−0.025	0.031	0.057	−0.013	0.034	0.040	0.004	0.008
Kurtosis (*zero mean*)													
143.51	6.06	3.95	3.67	3.24	3.48	3.50	3.45	3.23	3.40	3.55	3.58	3.48	3.32
149.93	4.71	3.52	3.34	3.11	3.18	3.19	3.35	3.30	3.04	3.21	3.22	3.25	3.23
154.18	4.09	3.32	3.29	3.05	3.10	3.11	3.20	3.19	3.11	3.12	3.14	3.12	3.11
158.84	3.48	3.16	3.18	3.03	3.10	3.11	3.12	3.14	3.04	3.11	3.13	3.07	3.05
162.82	3.05	3.04	2.97	2.90	2.88	2.88	2.99	2.99	2.85	2.89	2.89	2.96	2.95

samples, prior to applying the FFT algorithm which gave a frequency resolution of 0.73 Hz, and an overlap of 70% was used.

The spectrum levels of sound pressure for each of the four panels located in the PWT using spring supports are shown in Fig. 10. The results are from one test out of the total of five carried out for each panel, and the levels for each test and for all four panels were found to be within 3 dB OASPL, indicating a high degree of consistency. In each case the spectrum level, as opposed to the OASPL, was calculated using

$$S_{pp}(f) = 10\log_{10}\frac{p_{\Delta f}^2/\Delta f}{p_{ref}^2}, \tag{1}$$

where $p_{\Delta f}^2/\Delta f$ is the average spectral density of pressure in the band Δf, and p_{ref} is the reference pressure equal to 2×10^{-5} Pa (the threshold of human hearing). As can be seen from Fig. 10, the

Table 9
Statistical properties for panel 4 subject to random acoustic excitation in the PWT

OASPL (dB)	Mic. (Pa)	Acc.1 ($N\,m^{-1}s^2$)	Acc.2 ($N\,m^{-1}s^2$)	gi1 (με)	gi2 (με)	gi3 (με)	gi4 (με)	gi5 (με)	go1 (με)	go2 (με)	go3 (με)	go4 (με)	go5 (με)
Mean													
143.20	−7.46	−0.0004	0.0003	9.87	6.86	8.58	12.90	15.74	−2.11	−1.12	−8.91	−6.75	−3.77
149.49	−7.34	−0.0004	0.0003	18.45	14.61	15.47	20.99	24.71	−3.53	−2.59	−11.68	−9.84	−5.92
154.69	−7.64	−0.0004	0.0003	24.27	20.46	20.46	26.91	30.97	−4.05	−2.91	−12.28	−10.80	−6.62
159.49	−7.66	−0.0004	0.0003	32.14	27.90	26.90	34.15	39.31	−3.50	−2.62	−12.00	−10.73	−6.28
163.71	−7.44	−0.0004	0.0003	45.20	41.07	39.07	50.54	57.45	−3.86	−2.37	−11.30	−10.70	−6.00
Standard deviation (*r.m.s.*)													
143.20	289.34	0.004	0.014	5.91	15.17	18.15	4.11	4.86	5.76	7.28	7.47	9.91	10.13
149.49	596.34	0.009	0.032	10.70	36.11	43.36	8.54	9.83	12.58	16.42	17.09	21.36	20.43
154.69	1085.57	0.018	0.057	19.31	70.07	83.84	15.62	18.65	24.16	30.73	32.22	38.10	35.90
159.49	1887.95	0.034	0.102	35.73	134.35	158.96	28.37	35.29	46.13	56.52	59.39	65.95	62.24
163.71	3069.39	0.058	0.163	57.99	218.45	255.68	45.48	56.74	75.09	90.54	95.36	102.92	97.08
Skewness (*zero mean*)													
143.20	−0.087	−0.022	0.045	−0.031	0.059	0.029	0.056	0.072	0.000	−0.023	−0.017	0.004	−0.009
149.49	−0.098	0.014	0.106	0.002	0.035	−0.008	−0.036	0.038	−0.001	0.017	0.019	0.009	0.009
154.69	−0.037	0.031	0.117	−0.017	0.055	−0.002	−0.031	0.014	−0.012	−0.007	−0.004	−0.003	−0.017
159.49	−0.046	0.009	0.111	−0.053	0.041	−0.011	−0.020	0.000	0.023	−0.005	−0.009	−0.005	−0.016
163.71	−0.078	−0.001	0.111	−0.033	0.033	−0.001	−0.021	−0.020	0.005	−0.035	−0.031	−0.022	−0.028
Kurtosis (*zero mean*)													
143.20	4.76	3.63	3.54	3.20	3.40	3.35	3.25	3.00	3.21	3.35	3.37	3.39	3.32
149.49	4.40	3.33	3.42	3.17	3.24	3.21	3.32	3.22	3.20	3.25	3.23	3.14	3.14
154.69	3.71	3.28	3.28	3.10	3.11	3.09	3.12	3.06	3.10	3.12	3.12	3.05	3.05
159.49	3.16	3.10	3.13	2.93	2.87	2.89	2.95	2.89	2.94	2.92	2.92	2.92	2.92
163.71	2.94	3.05	3.16	3.07	3.02	3.04	2.98	2.97	3.01	3.05	3.05	2.98	3.00

spectrum levels are fairly constant, particularly across the 60–600 Hz band, where shaping was applied to the input spectrum to the siren.

Typical plots of power spectral density (PSD), phase and coherence (with respect to the reference microphone measurement) are shown for one gauge on each of the four panels in Figs. 11 and 12. Each resonance is indicated by a peak in the PSD response accompanied by a change in phase of approximately 180°. For all four panels, the first and third non-rigid-body modes of vibration, which were recorded during the free vibration tests, have not been measured in the PWT. This is to be expected since these modes were associated with torsional vibration of the panel, which was not excited in the PWT due to the symmetric pressure loading on the panels. With reference to Table 5, the measured response frequencies agree very well with the estimated natural frequencies obtained using the finite element models of the panels with spring supports included.

For the majority of the strain gauge measurements, the predominant response was in the fundamental mode (excited in the PWT), which was further highlighted when one plots the

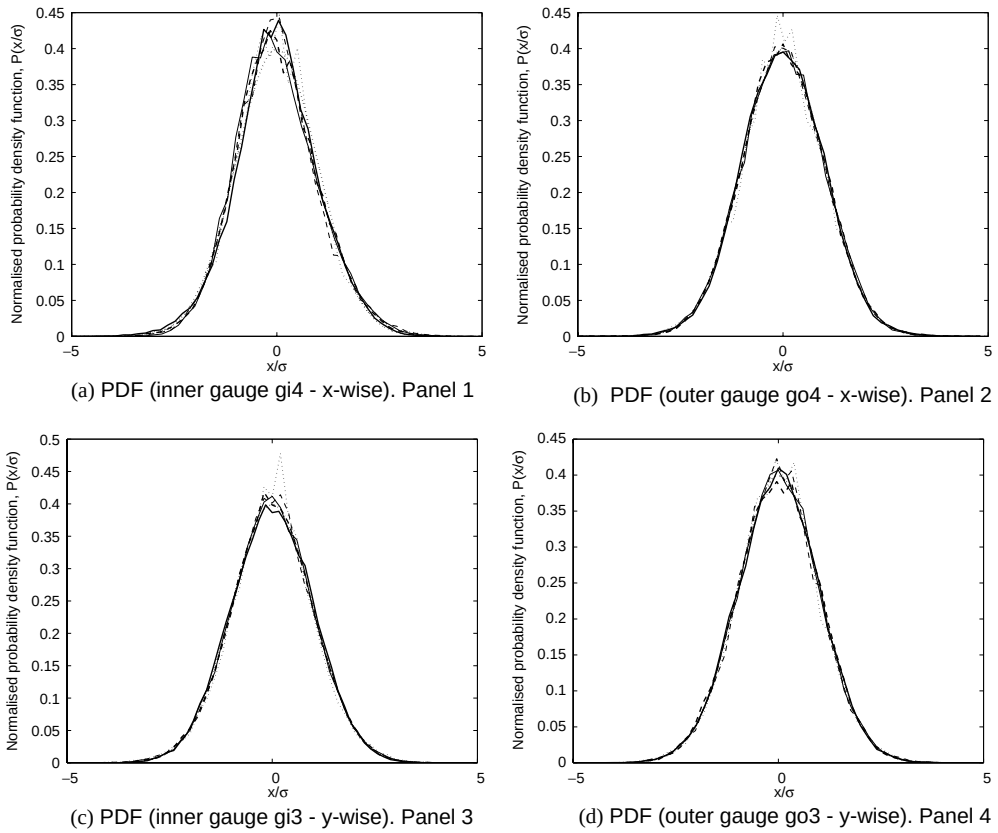

Fig. 8. Typical strain probability density functions for the four doubly curved panels (⋯, Gaussian; ⋯, 140 dB; - -, 145 dB; –, 150 dB; - -, 155 dB; -, 160 dB): (a) PDF (inner gauge gi4—x-wise), panel 1; (b) PDF (outer gauge go4—x-wise), panel 2; (c) PDF (inner gauge gi3—y-wise), panel 3; (d) PDF (outer gauge go3—y-wise), panel 4.

integral of the PSD versus frequency [21], as shown in Figs. 13–16 for the central gauges on each of the four panels. In this case, the integral across the PSD has been normalized with respect to the mean square response. These plots provide a very useful tool for the engineer interested in acoustic fatigue work, since they provide a means of assessing the percentage response of each of the measured modes of vibration. For the middle gauges of panels 1 and 2, approximately 80–90% of the total response was in the fundamental mode (first bending mode), whereas for panel 3, gauges gi4 and go4 (x-wise gauges) show that the fundamental mode accounts for approximately 40% of the response over the frequency band, and for panel 4, gauge go4, the fundamental mode accounts for approximately 20% of the total response. Panels 3 and 4 are particularly stiff in the x direction due to the high curvature along the short side (y direction), which could account for the lower response peak in the fundamental bending mode of vibration.

The overall r.m.s. strains for each of the 10 gauges, and for all four panels, are given in Tables 6–9 as the standard deviation, which is equal to the r.m.s. value when the mean is zero. These values are also plotted against the OASPLs as shown in Fig. 17. The highest r.m.s. strain was

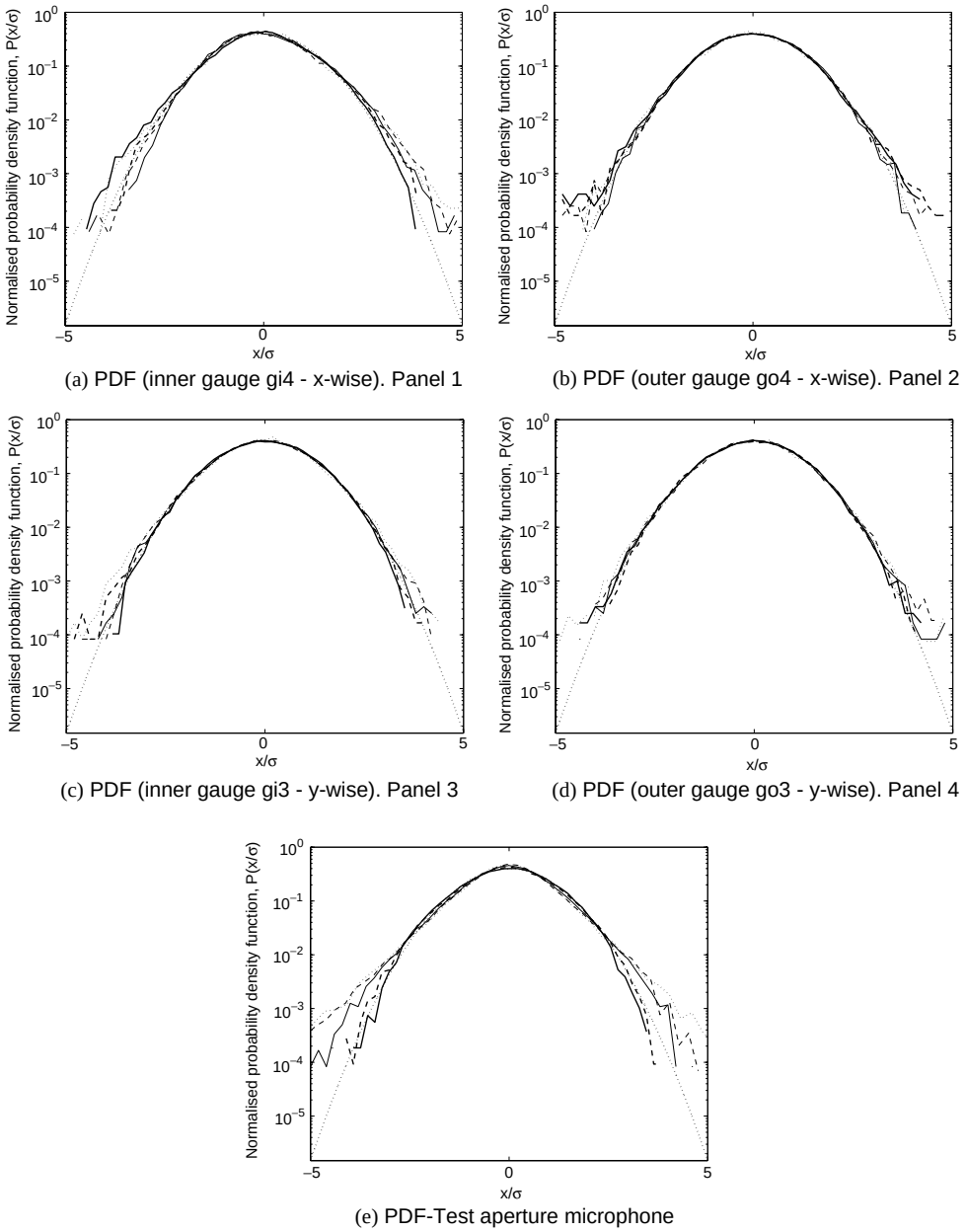

Fig. 9. Typical strain probability density functions for the four doubly curved panels and the test aperture microphone (logarithmic vertical axis) (···, Gaussian; ···, 140 dB; - -, 145 dB; –, 150 dB; - -, 155 dB; -, 160 dB): (a) PDF (inner gauge gi4—x-wise), panel 1; (b) PDF (outer gauge go4—x-wise), panel 2; (c) PDF (inner gauge gi3—y-wise), panel 3; (d) PDF (outer gauge go3—y-wise), panel 4; (e) PDF—test aperture microphone.

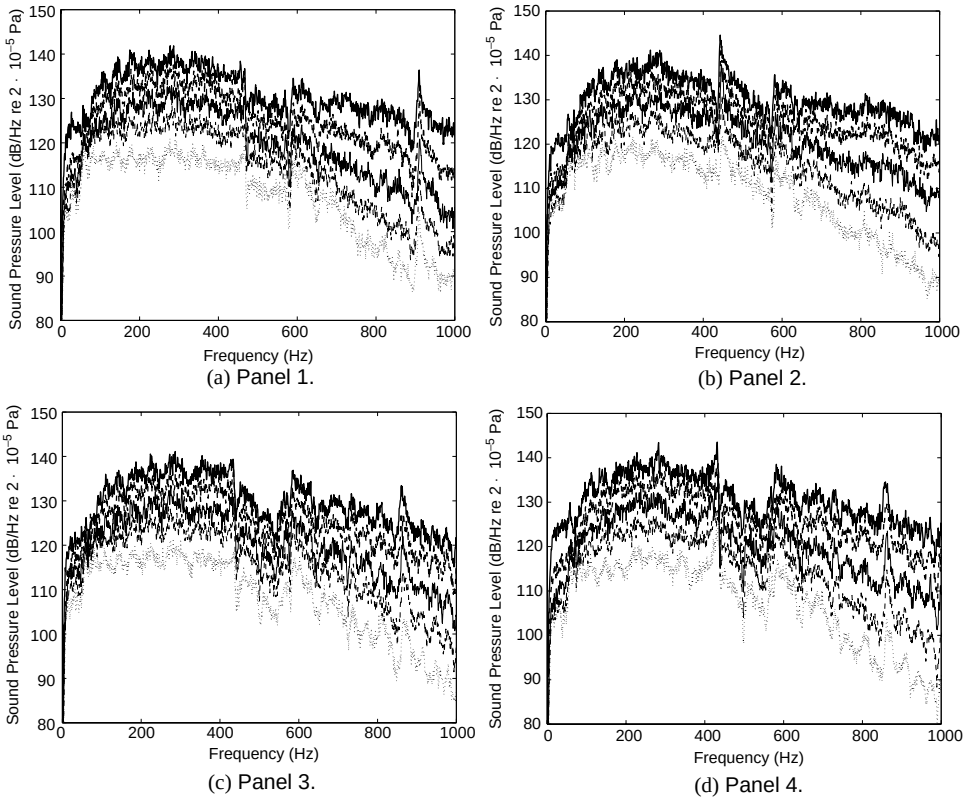

Fig. 10. Sound pressure level spectrum for each of the four test panels (OASPL runs ⋯, 140 dB; - -, 145 dB; –, 150 dB; - -, 155 dB; -, 160 dB): (a) panel 1; (b) panel 2; (c) panel 3; (d) panel 4.

measured at position gi3 on panel 4, which has an asymmetric lay-up with two face plate layers and six backing skin layers, in addition to which it is stiffer in the x direction due to the high curvature in the y direction. This result also corresponds with the result shown in Fig. 16 where for gauge go4, the fundamental bending mode only accounts for 20% of the total response, as mentioned previously. For panels 1 and 2, the highest strains were recorded at gauge locations go1 and go4, both x-wise gauges on the outer or backing skin. For panels 3 and 4, which are stiffer in the x direction, the highest strains were recorded by the two y-wise gauges gi2 and gi3, located on the inner or facing skin. Sweers [18] suggested that the strain at the centre of the backing skin will invariably be higher than that at the centre of the facing skin. This was proved following tests carried out on flat honeycomb panels with aluminium face plates, and was later shown to be the case in a study conducted by Soovere on flat honeycomb panels with CFRP face plates [14]. However, introducing double curvature into a panel can have a profound effect on the strains at the centre of the panel. The experiments conducted here have shown that for rectangular panels with a small radius on the short side (panels 3 and 4), the greatest strains were at central locations on the inner (facing) skin (referred to as the outer skin by both Sweers and Soovere).

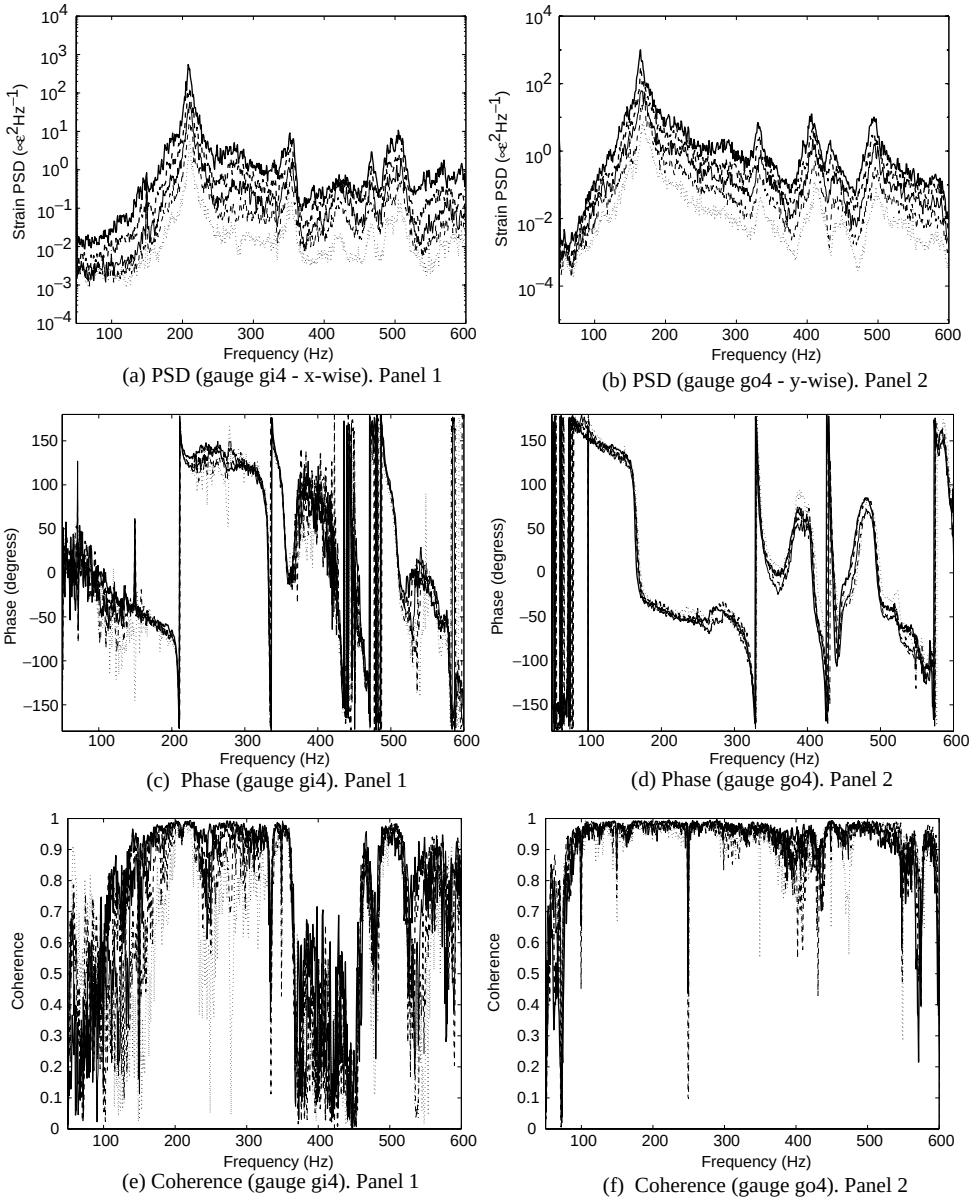

(a) PSD (gauge gi4 - x-wise). Panel 1
(b) PSD (gauge go4 - y-wise). Panel 2
(c) Phase (gauge gi4). Panel 1
(d) Phase (gauge go4). Panel 2
(e) Coherence (gauge gi4). Panel 1
(f) Coherence (gauge go4). Panel 2

Fig. 11. Typical plots of power spectral density, phase (w.r.t. ref. mic.), and coherence (w.r.t. ref. mic.) for panels 1 and 2 (OASPL runs ⋯, 140 dB; - -, 145 dB; –, 150 dB; - -, 155 dB; -, 160 dB): (a) PSD (gauge gi4—x-wise), panel 1; (b) PSD (gauge go4—y-wise), panel 2; (c) phase (gauge gi4), panel 1; (d) phase (gauge go4), panel 2; (e) coherence (gauge gi4), panel 1; (f) coherence (gauge go4), panel 2.

The outer-to-inner r.m.s. strain ratios are plotted in Fig. 18. The ratio for gauges 2 and 3 (the middle y-wise gauges) is between 0.8 and 0.9 for panels 1–3, whereas for panel 4 this ratio drops to between 0.4 and 0.5, possibly due to the asymmetric lay-up of the sandwich. For the x-wise gauges

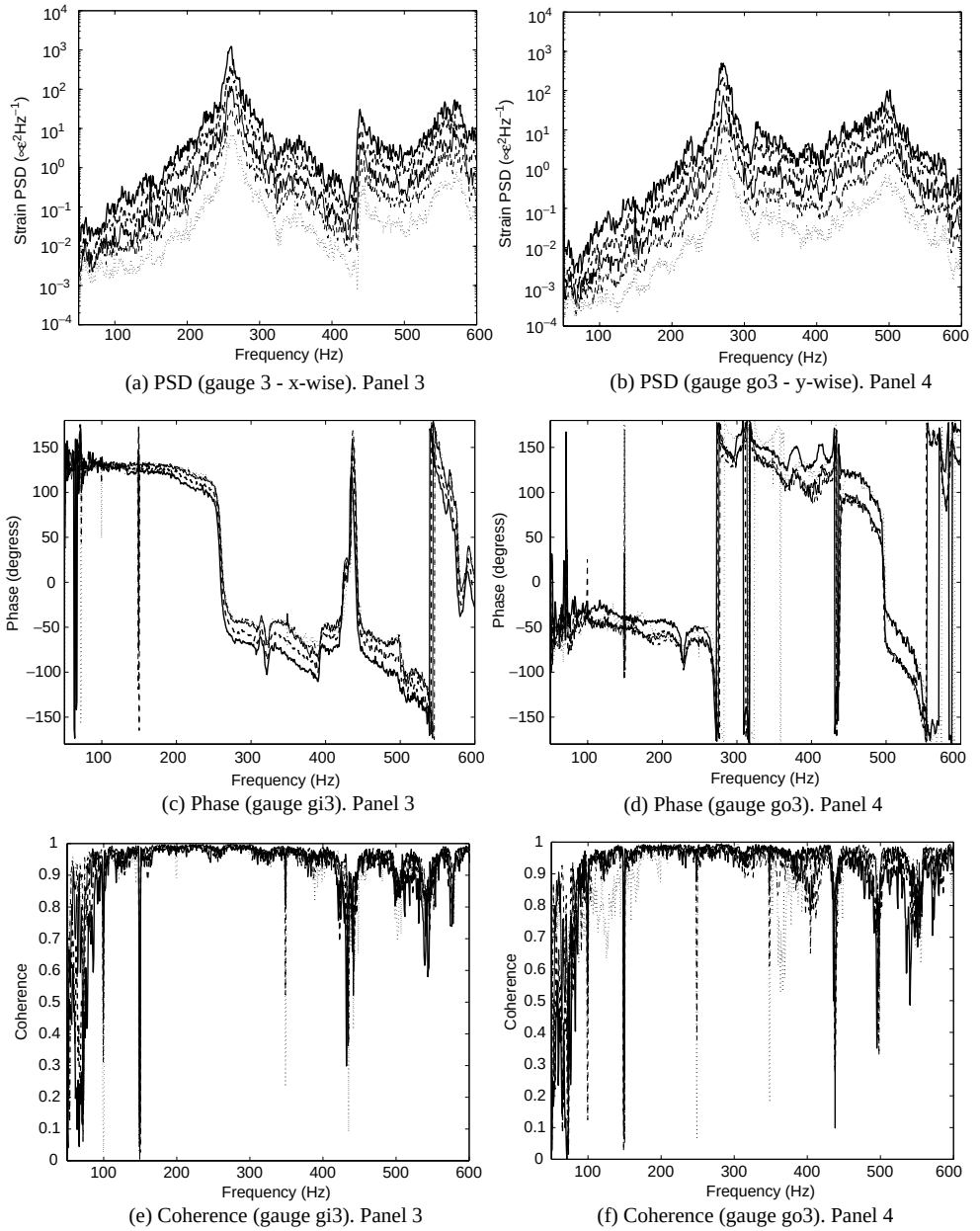

(a) PSD (gauge 3 - x-wise). Panel 3

(b) PSD (gauge go3 - y-wise). Panel 4

(c) Phase (gauge gi3). Panel 3

(d) Phase (gauge go3). Panel 4

(e) Coherence (gauge gi3). Panel 3

(f) Coherence (gauge go3). Panel 4

Fig. 12. Typical plots of power spectral density, phase (w.r.t. ref. mic.), and coherence (w.r.t. ref. mic.) for panels 3 and 4 (OASPL runs ⋯, 140 dB; - -, 145 dB; –, 150 dB; - -, 155 dB; -, 160 dB): (a) PSD (gauge gi3—x-wise), panel 3; (b) PSD (gauge go3—y-wise), panel 4; (c) phase (gauge gi3), panel 3; (d) phase (gauge go3), panel 4; (e) coherence (gauge gi3), panel 3; (f) coherence (gauge go3), panel 4.

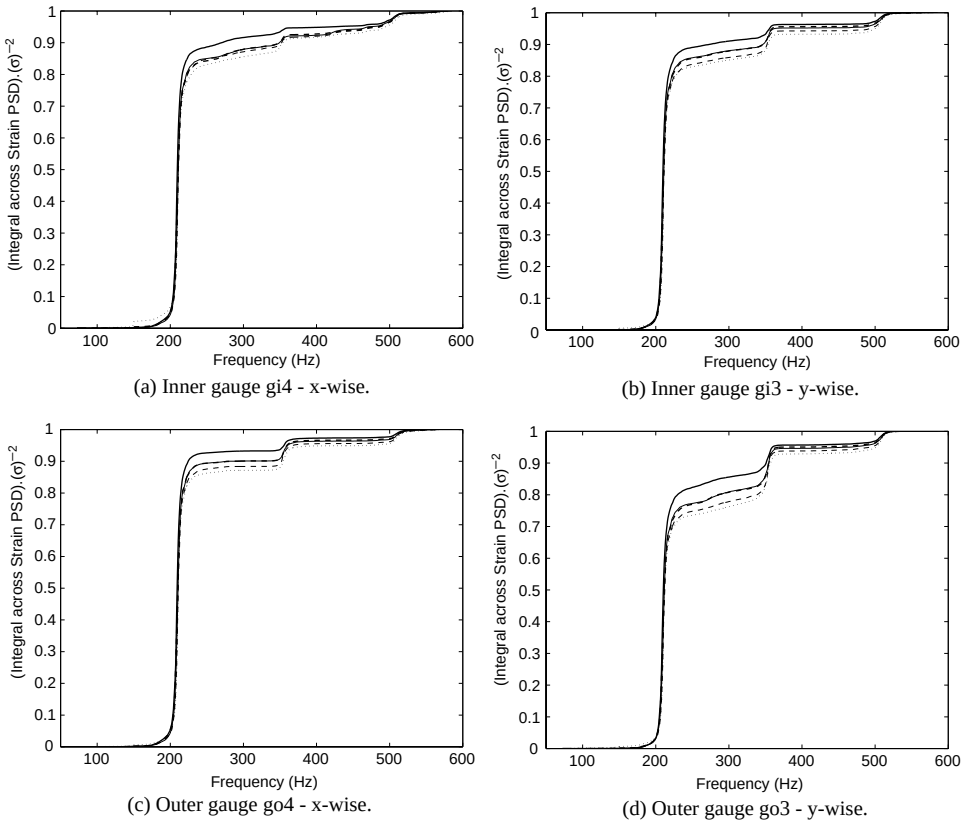

Fig. 13. Integral across the PSD for the inner strain gauges gi3 and gi4, and outer gauges go3 and go4, for panel 1 (OASPL runs ⋯, 140 dB; --, 145 dB; –, 150 dB; -- 155 dB; -, 160 dB): (a) inner gauge gi4—x-wise; (b) inner gauge gi3—y-wise; (c) outer gauge go4—x-wise; (d) outer gauge go3—y-wise.

4 and 5, the ratio is between 2.5 and 3 for panel 1, 1.2 and 1.4 for panel 2, 2.2 and 2.6 for panel 3 and 1.8 and 2.5 for panel 4. For flat rectangular honeycomb sandwich panels, a typical ratio of 2–2.5 has been quoted [18,17]. The ratios were found to be fairly constant with increasing OASPL, particularly for gauges 1 and 2.

4.1. Modal damping measurements

The modal, equivalent, viscous damping ratios for each of the four panels were obtained from the transfer function of strain/force using the half-power point method. The values are presented in Table 10, and will later be used in the forced response finite element models, which is presented in Part 2 of this study. These values are also compared with those obtained from the free vibration tests presented in a previous study [16]. It should be noted at this point that this comparison is only approximate. Although there was some agreement between the resonant response frequencies of the freely supported panels and the panels in the PWT aperture, the use of spring supports resulted in a 2–3% decrease in the first resonant response

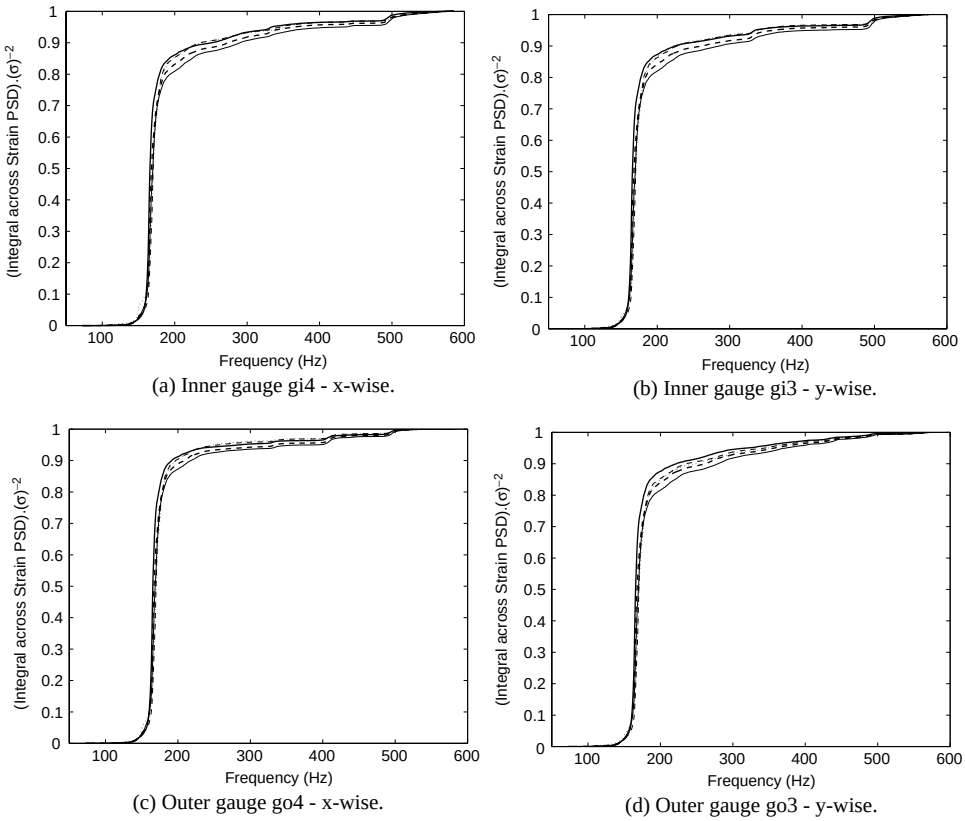

Fig. 14. Integral across the PSD for the inner strain gauges gi3 and gi4, and outer gauges go3 and go4, for panel 2 (OASPL runs ⋯, 140 dB; --, 145 dB; –, 150 dB; -- 155 dB; -, 160 dB): (a) inner gauge gi4—x-wise; (b) inner gauge gi3—y-wise; (c) outer gauge go4—x-wise; (d) outer gauge go3—y-wise.

frequency compared to that of the freely supported panels for the same approximate deflection shape. One would have expected that the introduction of spring supports would result in an increase in the fundamental resonant response frequency (which is evident when one examines the results produced by the FE model, reported in Table 5). However, the extra mass loading of the air in the PWT aperture could account for this decrease in the resonant response frequencies. The damping ratios for the fundamental mode obtained from the PWT tests are substantially higher than those obtained from the free vibration experiments. The nature of damping in composite honeycomb panels has been shown to be primarily due to acoustic radiation [14]. It has also been suggested that the influence of the PWT can result in an increase in the damping ratio of the fundamental mode due to acoustic impedence effects [14], particularly if the panel cross-sectional area exceeds that of the PWT aperture, which is certainly the case here. In addition, the use of duct tape around the periphery of the panels along a high curvature zone would also produce a significant increase in the modal damping ratio due to the viscoelastic effects of the tape. The significant increase in the damping of the fundamental mode suggests that both the impedence effects and the

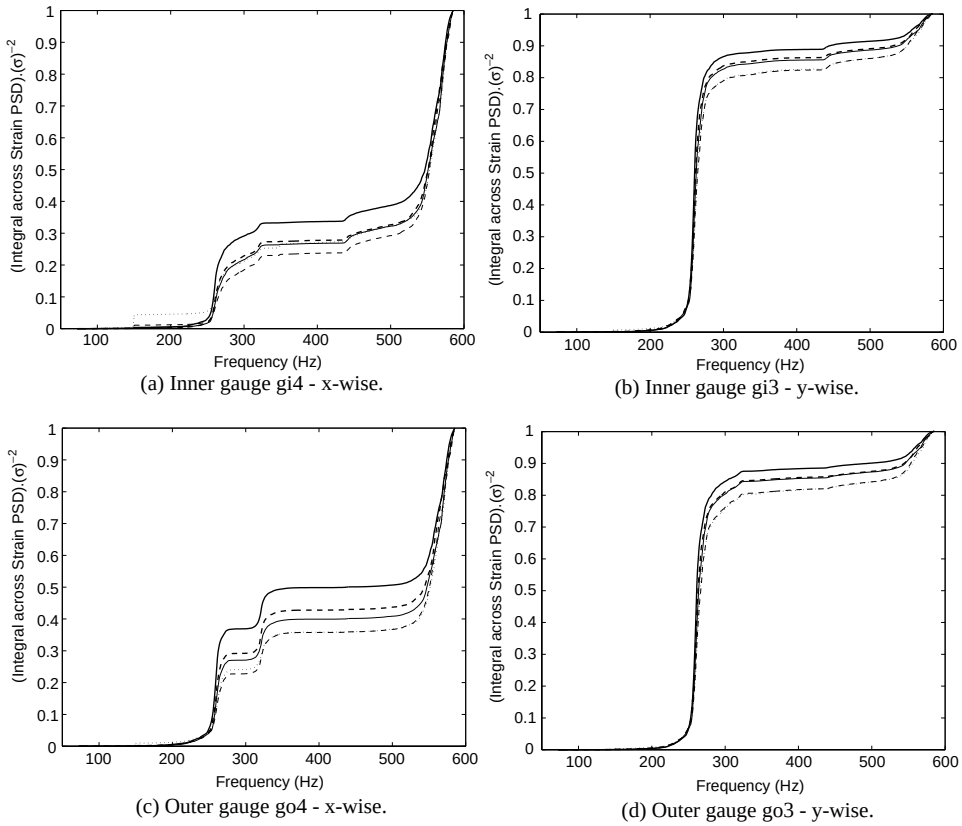

Fig. 15. Integral across the PSD for the inner strain gauges gi3 and gi4, and outer gauges go3 and go4, for panel 3 (OASPL runs ⋯, 140 dB; --, 145 dB; –, 150 dB; -- 155 dB; -, 160 dB): (a) inner gauge gi4—x-wise; (b) inner gauge gi3—y-wise; (c) outer gauge go4—x-wise; (d) outer gauge go3—y-wise.

application of duct tape around the periphery of the panels are the main contributory factors in this increase.

5. Summary

In this paper, the details of the high-intensity testing of a set of four doubly curved sandwich panels has been presented. The four test panels have been tested at levels from 142 to 164 dB, and the dynamic response has been measured using 10 strain gauges located on the inner (facing) skin and the outer (backing) skin, near to the centre and the edge of the panels. The results clearly show a linear response, at all sound pressure levels, and the statistics of the recorded signals have been shown to be Gaussian with skewness values close to zero and kurtosis values close to three. Not all of the modes excited during the free vibration experiments [16] were excited during the PWT tests due to the symmetric pressure load on the panels. Much of the response of the four panels was in the fundamental mode, which was clearly highlighted by the plots of the integral of

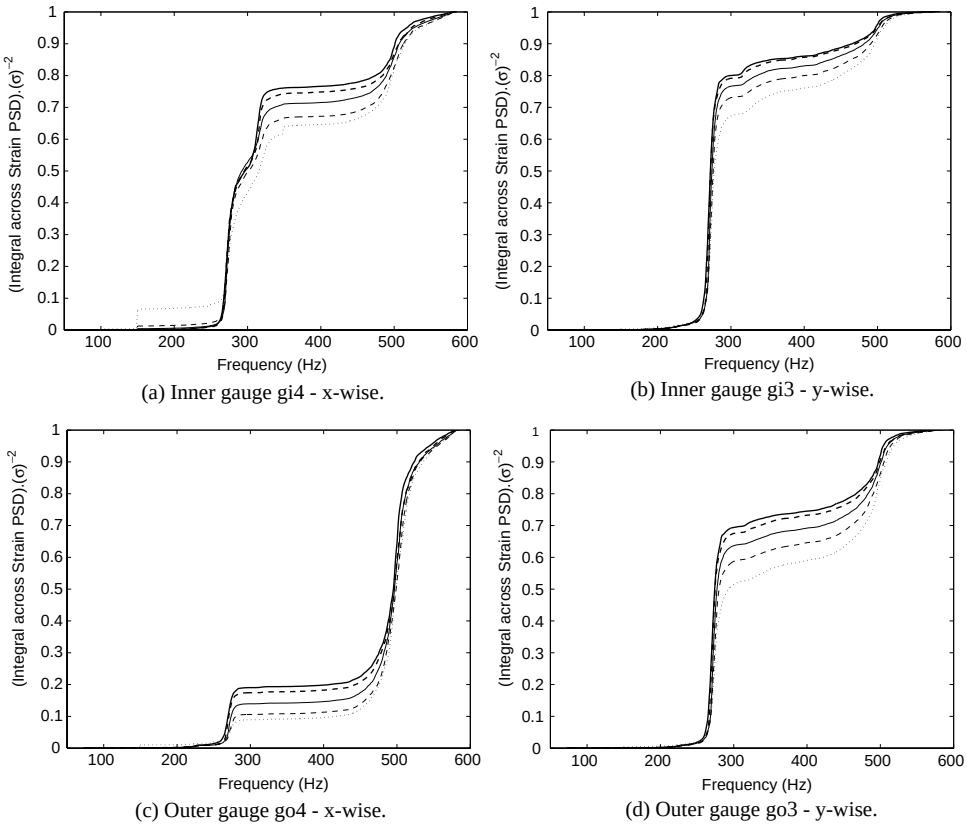

Fig. 16. Integral across the PSD for the inner strain gauges gi3 and gi4, and outer gauges go3 and go4, for panel 4 (OASPL runs ⋯, 140 dB; - -, 145 dB; –, 150 dB; - -, 155 dB; -, 160 dB): (a) inner gauge gi4—x-wise; (b) inner gauge gi3—y-wise; (c) outer gauge go4—x-wise; (d) outer gauge go3—y-wise.

the PSD across the frequency band. However, for panels 3 and 4, the fundamental mode accounted for between 20 and 40% of the total response for the outer x-wise near-centre gauge. The highest strains were recorded on the outer (backing) skin of panels 1 and 2. However, for panels 3 and 4, the highest strains were found to be on the inner (facing) skin. It follows that the introduction of double curvature, in this case a small short-side radius, can have a profound effect on the centre, or near-centre strains. Outer-to-inner r.m.s. strain ratios have also been presented, and have been found to be fairly constant with changing excitation level, particularly for gauges 1 and 2. The ratios for the symmetric sandwich configurations varied considerably from panel to panel. However for panel 1, which is the least curved of the panels, this ratio was between 2.5 and 3, which is consistent with the value of 2.5 quoted for flat rectangular sandwich panels [18,14].

Measured modal damping values have been presented and compared with those obtained from the vibration experiments [16]. The damping values for the fundamental mode were found to be substantially higher than the corresponding free vibration values, which has been attributed to the acoustic impedence effects introduced by the PWT aperture [14].

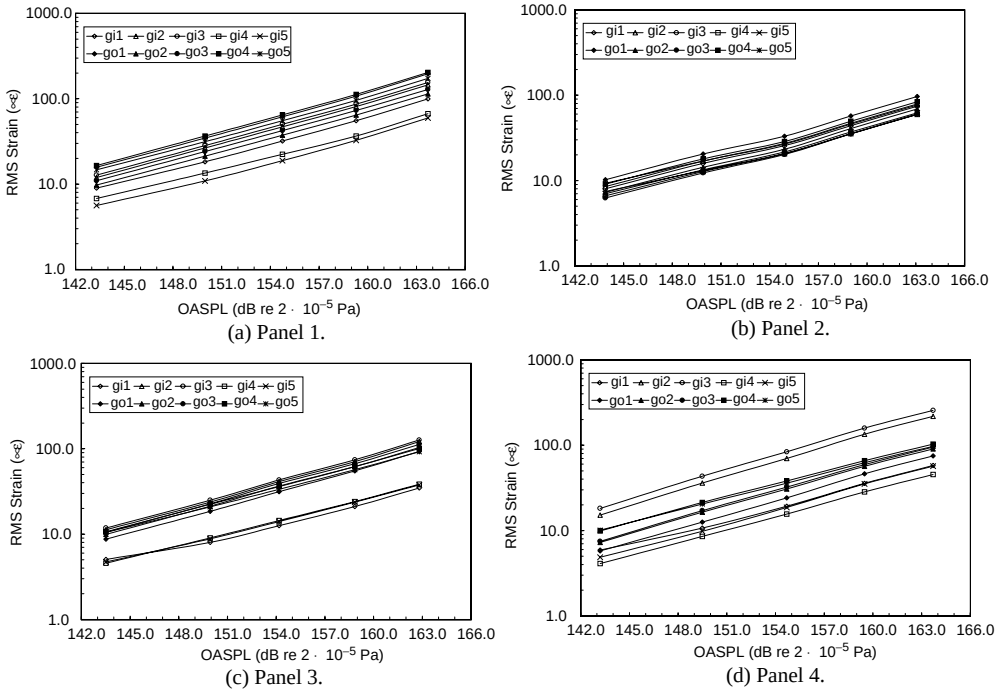

Fig. 17. Measured r.m.s. strain versus OASPL for the 10 strain gauges on all four panels: (a) panel 1; (b) panel 2; (c) panel 3; (d) panel 4.

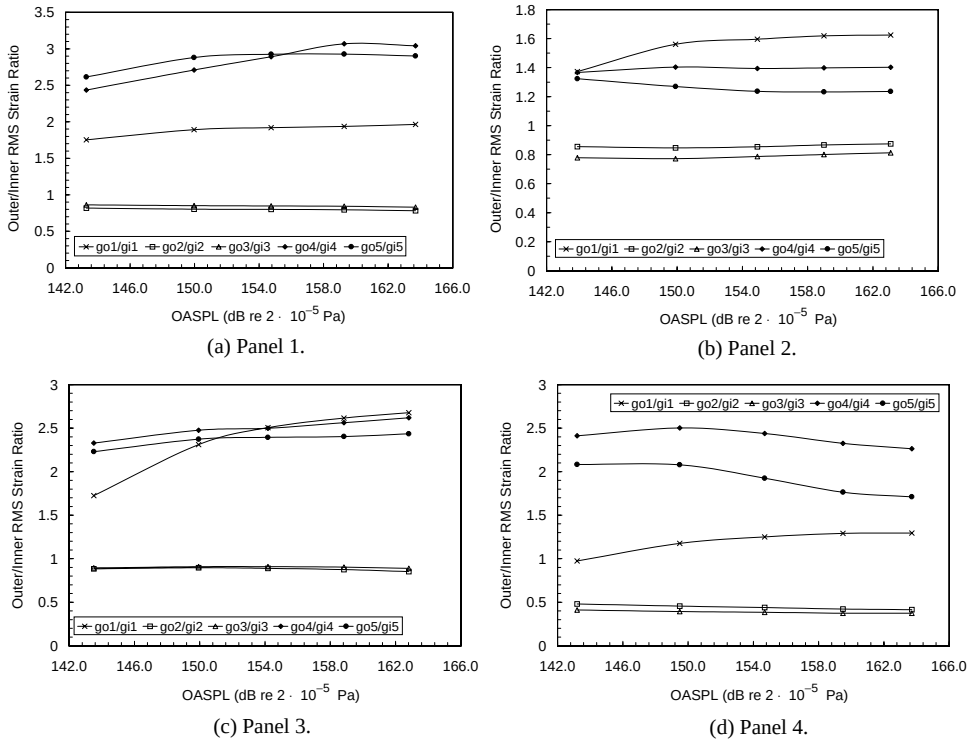

Fig. 18. Ratio of outer-to-inner r.m.s. strain for all four panels: (a) panel 1; (b) panel 2; (c) panel 3; (d) panel 4.

Table 10
Comparison of measured modal damping values obtained from the PWT tests and the free vibration tests

Panel	Frequency (Free) (Hz)	ζ_{free}	Frequency (PWT) (Hz)	ζ_{PWT}
1	214.6	0.0032	210.48	0.0105
	352.1	0.0098	353.9	0.0093
2	164.7	0.0039	163.1	0.0120
	343.1	0.0065	330.8	0.0084
3	264.5	0.0053	258.9	0.0125
	320.4	0.0148	320.7	0.0103
4	279.3	0.0059	269.6	0.0102
	312.4	0.0131	315.2	0.0124

Acknowledgements

This work was supported by the Engineering and Physical Sciences Research Council (EPSRC). The authors would also like to gratefully acknowledge the Institute of Sound and Vibration Research for the use of the PWT facility, and in particular Jim Baker and Dave Edwards of the University of Southampton for their technical assistance.

References

[1] B.L. Clarkson, Review of sonic fatigue technology, NASA Technical Report CP-4587, 1994.
[2] P.D. Green, Current and future problems in structural acoustic fatigue, AGARD Symposium, Impact of Acoustic Loads on Aircraft Structures, Lillehammer, Norway, 1994, pp. 1.1–1.5.
[3] E.J. Richards, D.J. Mead (Eds.), Noise and Acoustic Fatigue in Aeronautics, Wiley, New York, 1968.
[4] R.G. White, Developments in the acoustic fatigue design process for composite aircraft structures, Composite Structures 16 (1990) 171–192.
[5] R.W. Hess, R.W. Herr, W.H. Mayes, A study of the acoustic fatigue characteristics of some flat and curved aluminium panels exposed to random and discrete noise, NASA Technical Report TN D1, 1959.
[6] B.L. Clarkson, R.D. Ford, The response of a typical aircraft structure to jet noise, Journal of the Royal Aeronautical Society 66 (1962) 31–40.
[7] B.L. Clarkson, The design of structures to resist jet noise fatigue, Journal of the Royal Aeronautical Society 66 (1962) 603–616.
[8] B.L. Clarkson, Stresses in skin panels subjected to random acoustic loading, The Aeronautical Journal of the Royal Aeronautical Society 72 (1968) 1000–1010.
[9] L.D. Jacobs, D.R. Lagerquist, Finite element analysis of complete panel response to random loads, AFFDL Technical Report TR-68-44, 1968.
[10] N.R. Arcas, Prediction of stresses and fatigue life of acoustically excited aircraft structure, Shock and Vibration Bulletin 39 (2) (1969).
[11] A.G.R. Thompson, R.F. Lambert, The estimation of RMS stresses in stiffened skin panels subjected to random acoustic loading, AGARD-AG-162, Technical Report Section 5, 1972.

[12] J.R. Ballentine et al., Refinement of sonic fatigue structural design criteria, AFFDL Technical Report TR 67-156, 1968.
[13] M.J. Jacobson, Acoustic fatigue design information for fiber reinforced structures, AFFDL Technical Report TR 68-107, 1968.
[14] J. Soovere, Dynamic Response of Acoustically Excited Stiffened Composite Honeycomb Panels, Ph.D. Thesis, University of Southampton, 1984.
[15] I. Holehouse, Sonic fatigue of aircraft structures due to jet engine fan noise, Journal of Sound and Vibration 17 (3) (1971) 287–298.
[16] P.R. Cunningham, R.G. White, G.S. Aglietti, The effects of various design parameters on the free vibration of doubly curved composite sandwich panels, Journal of Sound and Vibration 230 (3) (2000) 617–648.
[17] J. Soovere, Random vibration analysis of stiffened honeycomb panels with beveled edges, American Institute of Aeronautics and Astronautics, Journal of Aircraft 23 (6) (1986) 537–544.
[18] J.E. Sweers, Prediction of response and fatigue life of honeycomb sandwich panels subjected to acoustic excitation, in: W.J. Trapp, D.M. Forney (Eds.), Acoustical Fatigue in Aerospace Structures, Syracuse University Press, Syracuse, NY, 1964, pp. 389–402.
[19] Y. Xiao, R.G. White, Development of design techniques for the avoidance of acoustic fatigue of box-like aircraft structures: sound pressure field measurement at the test section of the progressive wave tube facility, Technical Report, Department of Aeronautics and Astronautics, University of Southampton, Part 5, 1999.
[20] Bruel & Kjaer, B&K Spectrum Shaper Type 5612 Instruction Manual, DK-2850, 1977.
[21] R.G. White, A comparison of some statistical properties of the responses of aluminium alloy and CFRP plates to acoustic excitation, Composites 9 (1978) 251–258.